ACS APPLIED MATERIALS & INTERFACES

Research Article

www.acsami.org

Monitoring Cluster Ions Derived from Aptamer-Modified Gold Nanofilms under Laser Desorption/Ionization for the Detection of Circulating Tumor Cells

Wei-Jane Chiu,[†] Tsung-Kai Ling,[‡] Hai-Pang Chiang,[‡] Han-Jia Lin,[†] and Chih-Ching Huang*[,†,§,⊥]

[†]Department of Bioscience and Biotechnology, [‡]Institute of Optoelectronic Sciences, and [§]Center of Excellence for the Oceans, National Taiwan Ocean University, Keelung, 20224, Taiwan

[⊥]School of Pharmacy, College of Pharmacy, Kaohsiung Medical University, Kaohsiung 80708, Taiwan

Supporting Information

ABSTRACT: In this paper, we describe the use of pulsed laser desorption/ionization mass spectrometry (LDI-MS) for the detection of tumor cells through the analysis of gold cluster ions $[Au_n]^+$ from aptamer-modified gold nanofilms (Au NFs). We observed not only the transformation of the Au NFs into gold nanoparticles (Au NPs) but also the formation of gaseous gold cluster ions ($[Au_n]^+$; n = 1−5) under irradiation with a nanosecond pulsed laser. The size and density of the formed Au NPs and the abundance of $[Au_n]^+$ ions were both highly dependent on the thickness of the Au NFs (10−100 nm). Thin Au NFs tended to form highly dense Au NPs on the substrate and favored the desorption and ionization of gold cluster ions. The signal intensities of the $[Au_n]^+$ species, monitoring using mass spectrometry, decreased upon increasing the thickness of the Au NF from 10 to 100 nm and after modification with thiolated DNA. Furthermore, we found that Au NFs modified with mucin1-binding aptamer (Apt_{MUC1}−Au NFs) could selectively enrich MCF-7 cells (human breast adenocarcinoma cell line) in blood samples; coupled with LDI-MS analysis of the $[Au_n]^+$ ions, we could detect MCF-7 cells selectively in blood samples at abundances as low as 10 cells. This approach offers the advantages of high sensitivity, selectivity, and throughput for the detection of circulating tumor cells, and has great potential for use as a powerful analytical platform for clinical diagnoses of tumor metastasis.

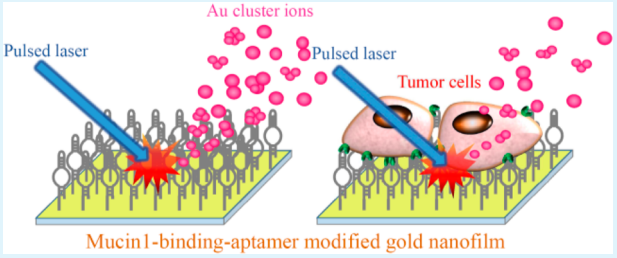

KEYWORDS: *nanofilms, nanoparticles, clusters, laser desorption/ionization, circulating tumor cells*

INTRODUCTION

The unique quantum confinement effects and thermal and chemical properties of two-dimensional nanofilms have been exploited for many applications, including integrated circuits, photodetectors, thermal conductive detectors, and biomedical devices.[1−3] Dewetting of metastable metallic thin films (<100 nm) from solid substrates is of great interest for the production and control of nanostructures.[4] Under pulsed-laser irradiation of sufficiently high power density, the surface temperature of a metallic thin film may reach its melting or boiling point, thereby transforming its structure.[5] It has been demonstrated that pulsed-laser irradiation can induce ultrafast thermal effects that can lead to the dewetting of metallic nanofilms and the formation of porous nanosubstrates, nanofilaments, nanoparticles (NPs), and/or self-organized nanopatterns.[5,6] Two possible routes for the transformation of metallic nanofilms into NPs (nanoislands) have been proposed: (i) heterogeneous nucleation from liquid phases located on defects or contaminants and (ii) rupture of the film as a result of hydrodynamic spinodal instability during thin film/spinodal dewetting.[7,8] Recently, spinodal dewetting has been demonstrated as having the most significant effect on the transformation of metallic nanofilms when irradiated with a nanosecond-pulsed laser.[9] The spinodal line represents the stability limit of a superheated unstable substance in the pressure−temperature phase diagram.[10] The homogeneous nucleation and growth of NPs from a nanofilm becomes spontaneous once the sample overcomes the free energy barrier.[11] After initiation of spinodal hydrodynamic dewetting, perturbations in the superheated thin liquid film grow over time, causing the film to become unstable; nanofilaments and/or NPs will then be formed once the intermolecular forces reach the same value as the surface tension force.[9,12] Film−substrate and film−film intermolecular interactions play vital roles during thin film spinodal dewetting.[9−13] Evaporation of the metal and the formation of metallic cluster ions in gaseous phase presumably accompany the transformation of the nanofilm,[14] yet most of the previously reported proposed mechanisms of nanofilm dewetting have assumed no losses of metal.[9−13] Although analyses of metallic cluster ions can

Received: January 26, 2015
Accepted: April 9, 2015
Published: April 9, 2015

DOI: 10.1021/acsami.5b00731
ACS Appl. Mater. Interfaces 2015, 7, 8622−8630

Scheme 1. Apt_{MUC1}–Au NFs for the Enrichment of Targeted and Detection Tumor Cells Coupled with LDI-MS

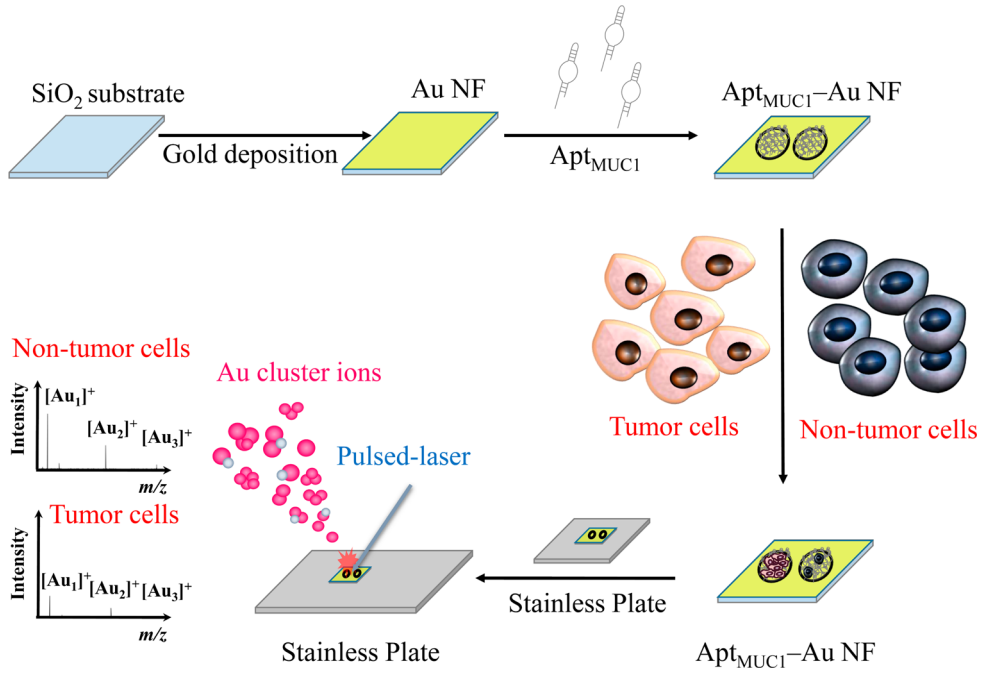

provide insight into the transformation mechanisms of nanofilm, related studies and applications are rare.[14,15]

Cancer is the second leading cause of death worldwide, with more than 90% of deaths in cancer patients attributable to metastasis. The early dissemination of tumor cells from tissue is usually undetectable in patients when performing conventional histopathological examinations.[16] Immunocytochemical and molecular assays have been developed recently for the specific detection of metastatic tumor cells in lymph nodes, peripheral blood, and bone marrow, prior to the manifestation of metastasis.[16] The detection and monitoring of circulating tumor cells (CTCs) is useful for prognosis, prediction of response to therapy, and guiding clinical decision-making for patients with localized or metastatic cancers.[17] CTCs are, however, extremely rare in extremely complex biological samples; that is, only a few hundred CTCs, out of more than 1×10^9 hematological cells, may be present in 1 mL of blood. In recent years, many optical and electrochemical techniques have been developed for the detection of CTCs in blood, after isolation and enrichment.[18] Although some of these techniques allow the selective detection of CTCs with ultrahigh sensitivity (several cells per milliliter of blood), they still have some setbacks, such as the requirement for complicated immobilization of recognizing ligands (e.g., antibodies) and tedious enrichment, separation and labeling processes. Although the throughput of pulsed-laser desorption/ionization mass spectrometry (LDI-MS) is much higher than those of analyses based on optical and electrochemical detection, LDI-MS has not been applied for CTC detection based on the best of our knowledge.

In this present study, we developed a simple LDI-MS–based approach for the detection of tumor cells in blood samples (Scheme 1). We prepared a chip featuring a gold nanofilm modified with mucin1-binding aptamer (Apt_{MUC1}–Au NF) for enrichment of MCF-7 cells (human breast adenocarcinoma cell line). MUC1 is a membrane glycoprotein (molecular weight: >200 kDa) that is often expressed in epithelial cells.[19] A variety of malignant tumors, including breast, gastric, and ovarian carcinomas, often feature the overexpression of MUC1.[19] Apt_{MUC1} (K_d: ca. 0.1 nM) from a systematic evolution of ligands by exponential enrichment (SELEX) process have been selected and employed it to recognize MUC1 units on the surfaces of the MCF-7 breast cancer cells.[20−25] In this study, we investigated the effects of the film thickness of the Au NFs, the laser power density, and the surface properties on the film's transformation and formation of Au cluster ions under nanosecond pulsed-laser irradiation. Furthermore, we have demonstrated that the Apt_{MUC1}–Au NFs could selectively enrich MCF-7 cells from blood samples and, when coupled with LDI-MS analysis, could allow the selective detection of these MCF-7 cells. Using our Apt_{MUC1}–Au NF/LDI-MS protocol with monitoring of the signals for Au cluster ions ($[Au_n]^+$), we could detect as few as 10 MCF-7 cells in blood samples. Although we have employed fibrinogen-modified gold nanoparticles/cellulose membrane for the detection of thrombin through monitoring the decrease in Au cluster ions after formation network fibrin structures on the membrane in our previous study.[26] Herein, we demonstrated the tumor cells can be simply enriched by functional Au NFs and coupled with high-throughput LDI-MS analysis could detection of CTCs. Our present approach appears to have great potential for application in clinical diagnoses of tumor metastasis.

EXPERIMENTAL SECTION

Chemicals. Tris(hydroxymethyl)aminomethane (Tris), hydrochloric acid, sodium chloride, potassium chloride, magnesium chloride, and calcium chloride were purchased from Mallinckrodt Baker (Phillipsburg, NJ, USA). Apigenin was purchased from Sigma–Aldrich (Milwaukee, WI, USA). Gold slugs (purity: ≥99%) were purchased from Fangather Tech (Taipei, Taiwan). SiO_2 cover glass substrates (22 × 22 mm; thickness: 0.15 mm) were purchased from Paul Marienfeld (Lauda-Königshofen, Germany). All thiolated DNA (sequences listed in Table S1 in the Supporting Information) were purchased from Integrated DNA Technologies (Coralville, IA, USA). Alpha-MEM cell medium and fetal bovine serum were purchased from GIBCO

DOI: 10.1021/acsami.5b00731
ACS Appl. Mater. Interfaces 2015, 7, 8622−8630

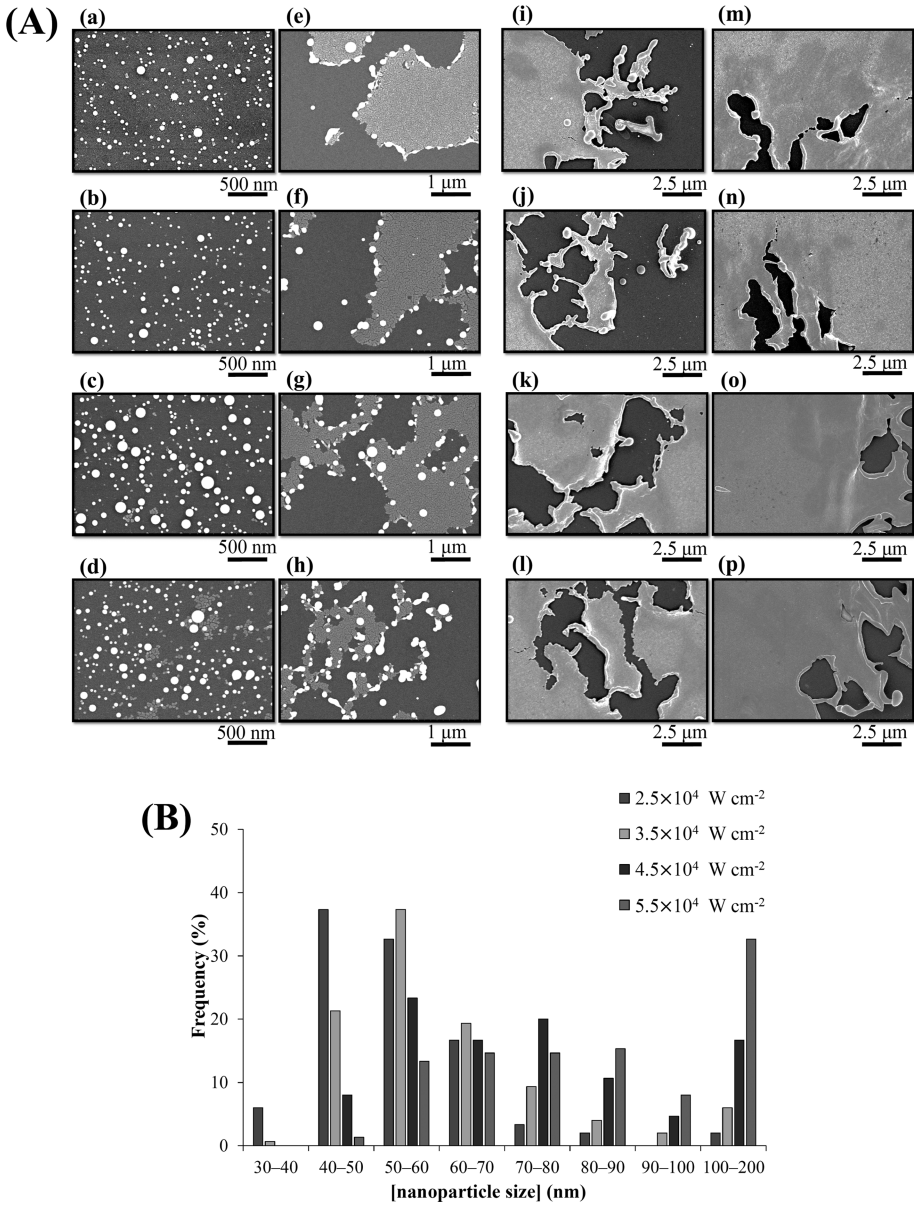

Figure 1. (A) Representative SEM images of (a–d) Au $NFs_{10\ nm}$, (e–h) Au $NFs_{20\ nm}$, (i–l) Au $NFs_{50\ nm}$, and (m–p) Au $NFs_{100\ nm}$ after irradiation with the 300 laser pulses at power densities of (a, e, i, m) 2.5×10^4, (b, f, j, n) 3.5×10^4, (c, g, k, o) 4.5×10^4, and (d, h, l, p) 5.5×10^4 W cm^{-2}. (B) Size distribution histograms of Au NPs formed from Au $NFs_{10\ nm}$ after irradiation with the 300 laser pulses at power densities ranging from 2.5×10^4 to 5.5×10^4 W cm^{-2}.

(Campinas, Brazil). Hoechst 33258 and prequalified human recombinant epidermal growth factor 1–53 (EGF 1–53) and bovine pituitary extract were purchased from Invitrogen (Carlsbad, CA, USA). MUC1 (VU4H5) mouse mAb was purchased from Cell Signaling Technology (Danvers, MA, USA). Five mM Tris-HCl buffer solution (pH 7.4) containing 150 mM NaCl, 5 mM KCl, 1 mM $MgCl_2$, and 1 mM $CaCl_2$ was used to mimic a physiological buffer solution; for simplicity, the concentration of this physiological buffer is denoted as 1×. Milli-Q ultrapure water (18 MΩ; Millipore, Billerica, MA, USA) was used in all experiments.

Preparation of the Au NF Chips and LDI-MS. Au NFs (10–100 nm) were deposited on SiO_2 cover glasses (22 × 22 mm) through thermal evaporation. Briefly, SiO_2 cover glasses (10 slides) were immersed in piranha solution [1:3 (v/v) 30% H_2O_2:H_2SO_4, 15 mL; ***CAUTION**: strongly corrosive*] in a glass Petri dish, incubated for 15 min, and then rinsed with copious amounts of water, followed by ethanol (EtOH). A thin film of Au was deposited on the SiO_2 cover glass substrates by using a thermal evaporator (EBX-6D, ULVAC, Inc. Japan), operated at 5.0×10^{-6} Torr, to electrically heat the Au source. The thickness was monitored in situ using a TM-350 thickness monitor (MAXTEK, Bad Ragaz, Switzerland). The as-prepared Au NFs chips were then attached to an LDI plate using adhesive polyimide film tape. Mass spectrometry was performed using an AutoflexIII LDI time-of flight (TOF) mass spectrometer (LDI-TOF MS; Bruker Daltonics, Bremen, Germany) operated in the reflectron positive-ion mode. The samples were irradiated with a SmartBeam laser (Nd:YAG, 355 nm; pulse width 6 ns; beam diameter ca. 50 μm) at a frequency of 100 Hz. Ions produced by laser desorption were stabilized energetically during a delayed extraction period of 200 ns and then accelerated through the TOF chamber in reflection mode prior to entering the mass analyzer. The available accelerating voltages were in the range from +20 to −20 kV. The instruments were calibrated with respect to the signals from the Au clusters ($[Au_n]^+$; n = 1–5). In total, 300 pulsed laser shots were applied to accumulate signals from 10 LDI target positions under laser power densities from 2.5×10^4 to 5.5×10^4 W cm^{-2}. Scanning electron microscopy (SEM)

DOI: 10.1021/acsami.5b00731
ACS Appl. Mater. Interfaces 2015, 7, 8622–8630

was performed using an HR-FESEM S-4800 instrument (Hitachi High-Technologies, Tokyo, Japan).

Thiolated-DNA-Modified Au NFs. For the preparation of Au NFs modified with single-stranded DNA, droplets (20 μL) of thiolated-polythymine oligonucleotide T_{45} DNA (SH-T_{45}; 0−10 μM) in 1× physiological buffer were placed separately on Au NFs and incubated for 24 h at room temperature; the Au NF chip was kept on a filter paper (wetted with physiological buffer 1X) in a closed Petri dish. The diameter of the droplet of the SH-T_{45} DNA solution on the chip was approximately 3 mm. The as-prepared T_{45}−Au NFs were rinsed with deionized (DI) water (ca. 3 mL) to remove any weakly adsorbed SH-T_{45} DNA. Subsequently, the chip was dried with an air gun (60 lb in^{-2}) for 1 min, and then attached to an LDI plate using adhesive polyimide film tape. The saturated density of the aptamers on Au NFs was 2.0×10^{13}−5.0×10^{13} molecules/cm^2 when the thiolated DNA was immobilized on gold surfaces in high ionic strength solutions (>100 mM NaCl).[27]

Cell Cultures. A breast tumor cell line (MCF-7), a transformed human embryonic kidneys cell line (293T), and an immortalized normal mammary epithelial cell line (MCF-10A) were purchased from American Type Culture Collection (Manassas, VA, USA). In brief, the MCF-7 and 293T cells were maintained in alpha-MEM containing 10% fetal bovine serum, whereas the MCF-10A cells were cultured in alpha-MEM supplemented with prequalified human recombinant EGF 1−53 and bovine pituitary extract. All cells were cultured in a humidified incubator at 37 °C under 5% CO_2.

After incubation of MCF-7 (ca. 5×10^5 cells mL^{-1}; 0.5 mL $well^{-1}$) in the culture medium for 24 h at 37 °C under 5% CO_2, the culture medium was replaced with the same medium (0.5 mL) containing apigenin (75 μM) to inhibit MUC1 expression. The cells were then incubated for another 72 h. The cells were carefully rinsed three times with physiological buffer 1X, followed by treatment with the Alamar Blue reagent (10-fold dilution, 0.5 mL/well) for 4 h. The fluorescence arising from the reduction of the dye by the live cells was measured using a fluorescence microplate reader (Synergy 4) from BioTek (Winooski, VT, USA), with an excitation wavelength of 545 nm and an emission wavelength of 590 nm. Because the fluorescence was directly proportional to the number of cells, it could be used to calculate cell viability, assuming 100% viability in the control set (media containing no apigenin).

Coupling Apt_{MUC1}−Au NFs with LDI-MS for Detection of MCF-7 Cells. Apt_{MUC1}−Au NF chips were prepared using the same method as that described above for the T_{45}−Au NFs chips. Cell solutions (20 μL; 10−1000 cells in alpha-MEM containing 10% fetal bovine serum) were cast onto Apt_{MUC1}−Au NF chips and incubated for 1 h at room temperature, and then washed with 1X physiological buffer (ca. 3 mL). Subsequently, the chips were air-dried for 30 min, attached to an LDI plate using adhesive polyimide film tape, and analyzed using LDI-TOF MS. The Apt_{MUC1}−Au NFs presenting bound MCF-7 cells samples were irradiated with a SmartBeam laser (Nd:YAG, 355 nm) at 100 Hz. Ions produced by laser desorption were stabilized energetically during a delayed extraction period of 200 ns and then accelerated through the TOF chamber in reflection mode prior to entering the mass-analyzer. In total, 300 pulsed-laser shots were applied to accumulate signals from 10 LDI target positions under a laser power density of 4.5×10^4 W cm^{-2}.

Analysis of Blood Samples Spiked with MCF-7 Cells. Whole blood samples from a healthy female adult (24 years old) were drawn from the vein into a BD Microtainer Capillary Blood EDTA-K3. MCF-7 cells (0−1000 cells) were spiked into whole blood and then diluted 10-fold in 1X physiological buffer solution. The MCF-7−spiked blood samples were cast onto the Apt_{MUC1}−Au NF chips, which were then incubated for 1 h at room temperature before being washed with 1× physiological buffer (ca. 3 mL). The Apt_{MUC1}−Au NFs presenting bound MCF-7 cells were then subjected to LDI-MS analysis as described above.

RESULTS AND DISCUSSION

Pulsed Laser-Induced Transformation of Au NFs. Figure S1 (Supporting Information) displays SEM images of the surface morphologies and thicknesses of as-prepared Au NFs on SiO_2 substrates prior to nanosecond pulsed-laser irradiation. The expected thicknesses of the grown Au NFs (10, 20, 50, and 100 nm) were monitored in situ using a quartz crystal sensor (INFICON TM-350 thickness monitor) during their thin film deposition processes. The average thicknesses of the four as-deposited Au NFs were 10.7 ± 1.2, 20.4 ± 2.1, 50.4 ± 3.2, and 101.2 ± 3.5 nm, respectively, estimated from the cross-sectional views of the SEM images in Figure S1B in the Supporting Information. Thus, the actual thicknesses were consistent with the expected ones. Therefore, for simplicity, herein we denote these as-prepared Au NFs chips as Au $NFs_{10\ nm}$, Au $NFs_{20\ nm}$, Au $NFs_{50\ nm}$, and Au $NFs_{100\ nm}$, respectively. Homogenous cracks in the Au NFs were evident prior to nanosecond pulsed laser irradiation (Figure S1C in the Supporting Information). Hemispherical Au clusters nucleated and coalesced initially at the onset of the deposition of the Au NFs, then grew laterally on the substrate; finally, cracks formed between the granular grains.[28] Moreover, we noted that increasing the thickness of the Au thin film on the SiO_2 glass substrate from 10 to 100 nm caused the Au granular grains to grow into large island grains.

Figure 1 presents SEM images of the Au NF chips after irradiation with a smartbeam Nd:YAG laser (300 pulses; wavelength: 355 nm; laser pulse width: 6 ns; beam diameter: ca. 50 μm; frequency 100 Hz) at power densities ranging from 2.5×10^4 to 5.5×10^4 W cm^{-2}. During nanosecond pulsed laser irradiation, Au thin films absorb the photon energy of the laser light, undergoing their transformation when the laser fluence reaches a threshold value.[9] The transformation of such films is governed by not only the pulsed laser fluence but also the ratio between the surface energies at the boundaries between the substrate and the metal and between the metal and the surrounding medium.[9,29] The surface temperature of a Au NF may reach the melting point (ca. 1300 K) or the boiling point (ca. 3000 K) if the power density of the nanosecond pulsed laser is sufficiently high. The threshold energy density required to reach the melting point of the Au NFs (thickness: >10 nm) increased upon increasing the film thickness, mainly because of rising energy losses from the increased reflection coefficient (R) and the presence of a thermal gradient in the direction normal to the film surface.[30] The total reflection coefficient of a Au NF can be calculated using the equation for the Fresnel reflection coefficient (eq 1)

$$R = (r_{12} + r_{23}e^{2i\beta})/(1 + r_{12} + r_{23}e^{2i\beta})^2 \quad (1)$$

Where

$$\beta = 2\pi(h/\lambda)n_g$$

and r_{12} and r_{23} are the reflection coefficients at the interfaces between the Au NF and the surrounding medium and between the SiO_2 substrate and the Au NF, respectively; h is the thickness of the Au NF; n_g is the refractive index of gold; and λ is the laser irradiation wavelength.[30] On the basis of the reflection coefficient equation, we would expect the total Au NF reflection coefficient for the laser wavelength to increase with respect to the film's thickness.

We observed the formation of Au NPs in the Au $NFs_{10\ nm}$ and Au $NFs_{20\ nm}$ chips; in contrast, shrinking and rolling-up

DOI: 10.1021/acsami.5b00731
ACS Appl. Mater. Interfaces 2015, 7, 8622−8630

transformations occurred, followed by disintegration, for the Au $NFs_{50\ nm}$ and Au $NFs_{100\ nm}$ chips. Melting of the Au NFs led to dewetting processes and the formation of isolated Au NPs on the substrate (Figure 1A, a–d), mainly following the Rayleigh instability mechanism. The formation of perfectly spherical Au NPs was due to the large difference in surface energy between the substrate and the metal.[12,31] The area density (N) of the formed Au NPs is strongly correlated to the thickness (h) of the Au NFs; it can be expressed as eq 2

$$N = (A_H/16\pi\gamma^3)h^{-4} - K_l \quad (2)$$

where A_H is the Hamaker constant (3.1×10^{19} J), γ is the surface tension of liquid gold at the melting point (ca. 1.2 N/m), h is the film thickness, and K_l is the correction coefficient for the NPs lost through evaporation.[32] Accordingly, we might expect the density of formed Au NPs to be lower from a thicker Au NF. Indeed, we detected almost no Au NPs after pulsed laser irradiation of Au $NFs_{50\ nm}$ and Au $NFs_{100\ nm}$ (Figure 1A).

It has been reported that the average particle diameter (D) of Au NPs formed from Au NFs, after nanosecond pulsed laser annealing, is strongly dependent on the film thickness ($D = (192\pi^2\gamma/A_H)^{1/3}h^{5/3}$) and weakly dependent on the laser fluence and the number of pulses.[32] We found, however, that the values of D of the Au NPs formed after Au $NFs_{10\ nm}$ had been irradiated with 300 laser pulses at power densities of 2.5×10^4, 3.5×10^4, 4.5×10^4, and 5.5×10^4 W cm^{-2} were 54.9 ± 9.7, 64.3 ± 15.5, 81.4 ± 25.5, and 100.1 ± 35.0 nm, respectively (Figure 1B). The slight increases in the average sizes of the Au NPs after irradiation at higher power densities were probably due to partial evaporation and fragmentation of the smaller NPs, thereby increasing the mean size of the remaining ones.[9] We will prove this suggestion in a subsequent study. Notably, the abundance of larger Au NPs (100–200 nm) was higher after we had irradiated Au $NFs_{10\ nm}$ with the pulsed laser at a higher power density, presumably because adjacent nucleated NPs melted and fused to form larger NPs.

Generation of Au Cluster Ions. We observed that the pulsed laser not only induced the melting of Au NFs but also their evaporation and ionization. It is established that Au cluster ions can be produced under pulsed laser irradiation of Au NFs if the laser-generated energy overcomes the critical energy deficit of the Au NFs.[33] Figure 2A displays the mass spectra of Au NFs (thicknesses: 10–100 nm) recorded during nanosecond pulsed laser irradiation, revealing signals for the produced Au cluster ions ($[Au_n]^+$; n = 1–5). The ablation of Au NFs under irradiation with a nanosecond pulsed laser probably follows a photothermal evaporation mechanism,[34] in which absorption of laser energy by the Au NF leads to formation of Au NPs via spinodal dewetting, followed by surface melting, and eventually a decrease in size or splitting, due to evaporation from surface atoms or the entire particle. The formation of Au cluster ions during the evaporation of Au NFs is accompanied by electron ejection.[35] In the photothermal evaporation model, the degree of surface evaporation depends on the thermal energy transfer, temperature, and evaporation point of the Au NFs.[33−35] We found that the signal intensities of the Au cluster ions decreased upon increasing the thickness of Au NFs from 10 to 100 nm. It has been demonstrated that the evaporation points of a Au NF is highly dependent on the evaporation pressure and thickness of the film.[35−37] The evaporation efficiency (E_{eva}) can be expressed as eq 3

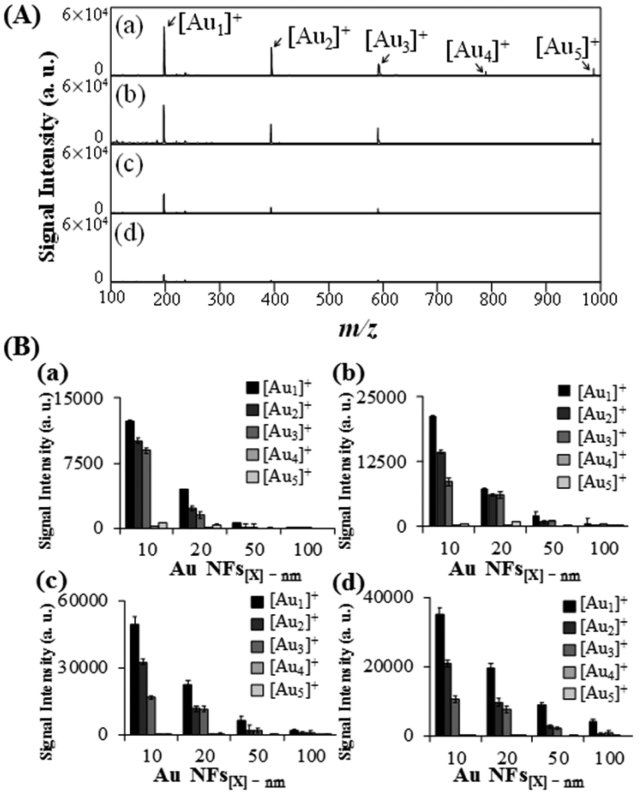

Figure 2. (A) Representative LDI-MS spectra of (a) Au $NFs_{10\ nm}$, (b) Au $NFs_{20\ nm}$, (c) Au $NFs_{50\ nm}$, and (d) Au $NFs_{100\ nm}$ under pulsed laser irradiation (300 pulses) at a power density of 4.5×10^4 W cm^{-2}. (B) Signal intensities of $[Au_n]^+$ (n = 1–5) ions recorded through Au NFs/LDI-MS at laser power densities of (a) 2.5×10^4, (b) 3.5×10^4, (c) 4.5×10^4, and (d) 5.5×10^4 W cm^{-2}. The signals at m/z 196.967, 393.933, 590.900, 787.866, and 984.83 in (A) represent the $[Au_1]^+$, $[Au_2]^+$, $[Au_3]^+$, $[Au_4]^+$, and $[Au_5]^+$ ions, respectively. Error bars in B represent standard deviations from three repeated experiments.

$$E_{eva} = \int_0^t \sqrt{\frac{M}{2\pi RT}}\frac{P(T)}{\pi\rho D h^2}dt \quad (3)$$

where M is the gold molar mass, R is the universal gas constant, T is a temperature, $P(T)$ is the temperature-dependent vapor pressure of gold, ρ is the density of gold, D is the diameter of a Au NP, and h is the thickness of the Au NF.[9] The intensities of the Au cluster ions formed from the Au NFs decreased upon increasing the thickness of the Au NFs, with similar trends observed upon varying the power of the laser irradiation (Figure 2B). The thicker Au NFs possessed higher boiling (evaporation) thresholds under pulsed laser irradiation. Moreover, higher reflection coefficients meant that the thicker Au NFs did not absorb as much laser energy, thereby producing lower abundances of Au cluster ions.

Effect of DNA Surface Covering. Next, we investigated the formation of Au cluster ions from various T_{45} DNA–modified Au $NFs_{20\ nm}$ chips. We prepared the T_{45}–Au $NFs_{20\ nm}$ samples by casting various concentrations (0–10 μM; 20 μL) of thiolated T_{45} DNA onto Au NFs, incubating for 24 h, and then washing the T_{45}–Au $NFs_{20\ nm}$ chips with DI water. We selected Au $NFs_{20\ nm}$ for this study because its Au cluster ion intensity and reproducibility were superior to those of the other Au NFs (Figure 2B). The signal intensities of the Au cluster ions decreased upon increasing the concentration of HS-T_{45} DNA from 0 to 10 μM (Figure 3A). We suspect that the thin

DOI: 10.1021/acsami.5b00731
ACS Appl. Mater. Interfaces 2015, 7, 8622–8630

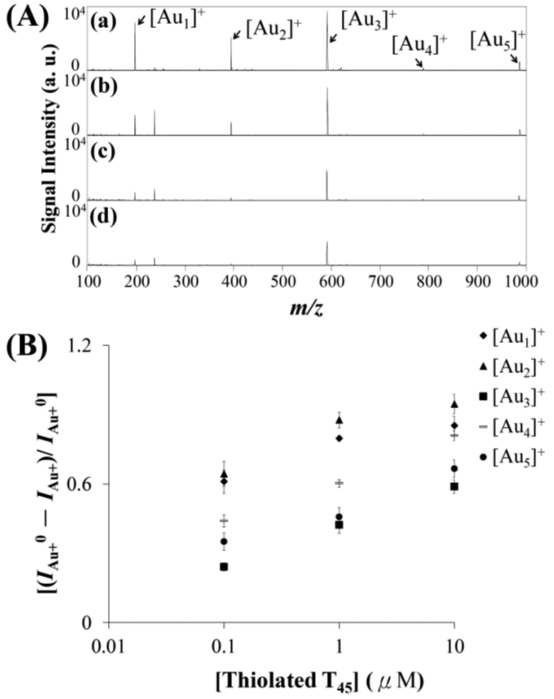

Figure 3. (A) Representative LDI-MS spectra recorded from Au $NFs_{20\ nm}$ modified with thiolated T_{45} DNA at concentrations of (a) 0, (b) 0.1, (c) 1.0, and (d) 10 μM. (B) Relative signal intensity of $[Au_n]^+$ ions $[(I_{Au+}{}^0 - I_{Au+})/I_{Au+}{}^0]$ plotted with respect to the concentration of thiolated T_{45} DNA. A total of 300 pulsed laser shots were applied under a laser power density of 4.5×10^4 W cm^{-2}. Error bars in B represent standard deviations from three repeated experiments.

film of Au transferred its absorbed laser energy to the surface T_{45} DNA molecules; as a result, the temperature of the Au NF decreased and evaporation of its surface atoms was suppressed, decreasing the intensity of the signals of the Au cluster ions in the mass spectrum. In addition, competitive ionization of the DNA molecules and the Au clusters, and complicated reactions between Au clusters ions and DNA fragments in the gas phase, might also have decreased the intensities of the signals for the Au cluster ions. From the relative decrease in the signal intensity of the Au cluster ions $\{(I_{Au+}{}^0 - I_{Au+})/I_{Au+}{}^0$; where $I_{Au+}{}^0$ and I_{Au+} represent the signal intensities of $[Au_n]^+$ ions in the absence and presence of T_{45} DNA, respectively$\}$ in the presence of T_{45} DNA, we conclude that the smaller Au cluster ions ($[Au_1]^+$ and $[Au_2]^+$) were more sensitive to the density of surface T_{45} DNA ligands (Figure 3B). The dense coverage of self-assembled T_{45} DNA on Au $NFs_{20\ nm}$ might have inhibited electron ejection from the Au NFs, thereby suppressing the fragmentation of the Au NPs into smaller positively charged Au clusters ions.[38]

Relative to matrix-assisted laser desorption/ionization mass spectrometry (MALDI-MS), surface-assisted laser desorption/ionization mass spectrometry (SALDI-MS) is an organic matrix-free approach that uses nanosubstrate materials or nanoparticles (NPs) to mediate the desorption process.[39] SALDI-MS possesses several advantages over MALDI-MS, including ready preparation of homogeneous samples, tolerance high salt, and low background noise. Despite the advantages of SALDI and the promising results achieved with nanoparticles-assisted LDI,[40−43] when nanoparticles are pipetted onto the target plate and air-dried at room temperature prior to MS analysis, their resulting inhomogeneous distribution inevitably leads to poor sample-to-sample reproducibility (RSD ≈ 10−30%). In the case of our approach, the Au NF as a substrate (Figure S1, Supporting Information) can provide greater reproducibility (RSD <15%; Figure 3B) than MALDI-MS, SALDI, and nanoparticles-assisted LDI approaches due to its highly homogeneous surface and can produce stable detectable signals for $[Au_n;\ n = 1-5]^+$ cluster ions in the MS analysis under laser irradiation.

We recorded SEM images (Figure S2A, Supporting Information) of the Au NPs remaining on the T_{45}−Au $NFs_{20\ nm}$ substrates after irradiating them with 300 laser pulses (4.5×10^4 W cm^{-2}). The distribution of particle diameters shifted to larger ones, with the particle densities increasing, upon increasing the content of deposited T_{45} DNA, presumably because the Au NPs readily fragmented into smaller ones and/or split from the substrates in the absence of surface T_{45} DNA. This result supports the notion that the surface T_{45} DNA ligands inhibited the formation of Au cluster ions. To the best of our knowledge, this paper reports the first observations of the evaporation of metallic cluster ions and the content of NPs remaining on the substrates both being highly dependent on the coverage of the surface ligands on the thin films during pulsed laser irradiation. Our findings suggest that the surface properties of a metallic thin film can be characterized by LDI-MS through monitoring of its cluster ions.

Using Apt_{MUC1}−Au NFs to Detect Tumor Cells. We employed the Apt_{MUC1}−Au NF chip as a capture probe for the detection of tumor cells, functioning based on the specific interactions between Apt_{MUC1} and MUC1 proteins on tumor cell surfaces and the changes in the intensities of Au cluster ions in LDI-MS analysis after the tumor cells had bound to the Au NF chip. Once the Apt_{MUC1}−Au NF chip had captured human breast adenocarcinoma MCF-7 cells, its Au NF absorbed less energy when exposed to laser pulses and transferred some of this absorbed laser energy to the surface cells. As a result, the evaporation of Au atoms was suppressed, leading to decreased intensities of the signals for the Au cluster ions in the mass spectra (Figure 4b). In the control experiment (Figure S3, Supporting Information), we found that the Apt_{MUC1}−Au NF chip's efficiency at capturing the MCF-7 cells was much higher than that of the T_{45}−Au NF chip, consistent with specific Apt_{MUC1}−MUC1 interactions enhancing the enrichment of MCF-7 cells. We also applied our Apt_{MUC1}−Au NFs/LDI-MS method to analyze other cells, namely normal mammary epithelial MCF-10A cells (Figure 4c) and transformed embryonic kidney 293T cells (Figure 4d). Relative to MCF-7 cells, the relative decreases in the $[Au_n]^+$ signal intensities were smaller for the MCF-10A cells (Figure 4c). Although MUC1 is expressed widely by normal epithelial cells, such as MCF-10A, its expression increases significantly when the cells become malignant (e.g., in breast tumors).[44] The MUC1 protein is, however, expressed aberrantly in some solid tumor cell lines; for example, the 293T cell line is a well-known MUC1-negative cell line.[45] The statistical significance of the responses [P-values (P) of 0.05 or less] obtained for the MCF-7 cell line or other cell lines have been shown in Figure 4B. Our results reveal the difference in relative decreases in the $[Au_n]^+$ signal intensities for MCF-7 cells with respect to control or other cells (MCF-10A cells and 293T cells) are significant ($P \leq 0.01$).

Next, we applied our Apt_{MUC1}−Au NF/LDI-MS system to the analysis of MCF-7 cells after treatment with apigenin (75 μM) for 72 h. Apigenin, a natural polyphenol product belonging to the flavone class, is present abundantly in some

DOI: 10.1021/acsami.5b00731
ACS Appl. Mater. Interfaces 2015, 7, 8622−8630

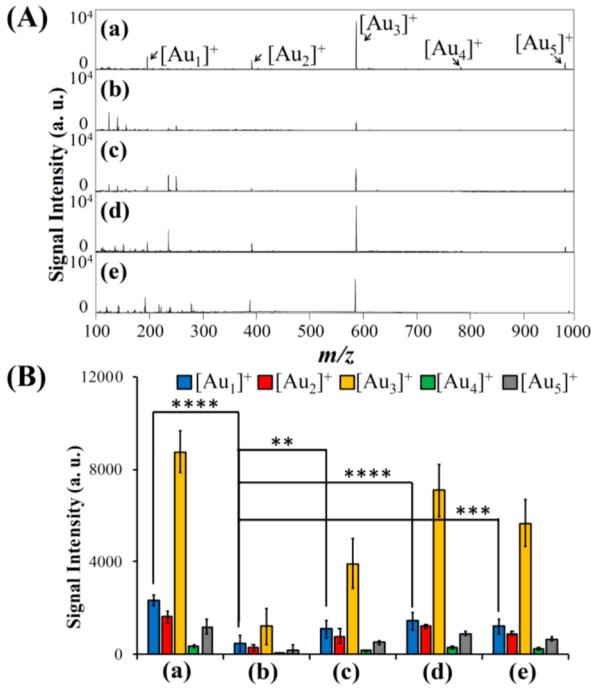

Figure 4. (A) Representative LDI-MS spectra and (B) corresponding MS intensities of Au cluster ions recorded from the Apt_{MUC1}–Au $NF_{20\ nm}$ substrate in the (a) absence and (b–e) presence of (b) MCF-7 (1000 cells), (c) MCF-10A (1000 cells), and (d) 293T (1000 cells) and (e) apigenin (75 μM)-treated MCF-7 (1000 cells). Error bars in B represent standard deviations from three repeated experiments. Stars indicate significant difference from the different cell lines with $^{**}P \leq 0.01$, $^{***}P \leq 0.001$ and $^{****}P \leq 0.0001$. Other conditions were the same as those described in Figure 3.

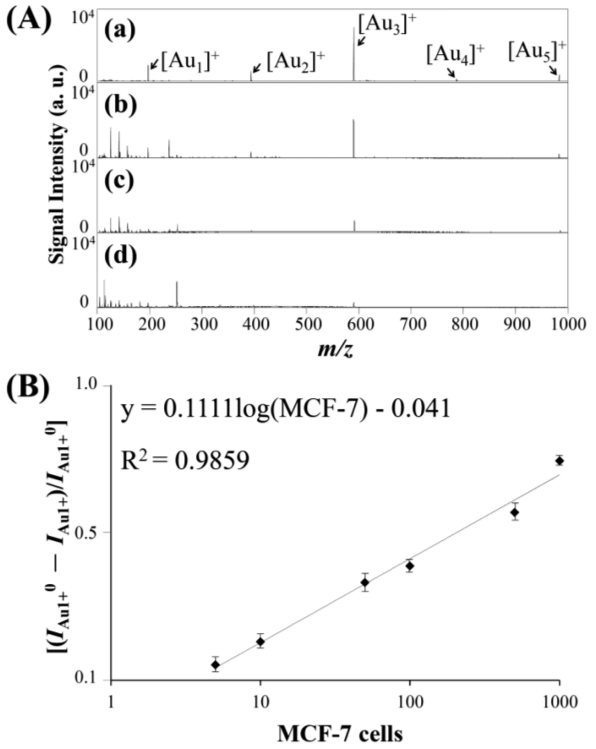

Figure 5. (A) LDI-MS spectra recorded using the Apt_{MUC1}–Au NF as a probe for the detection of (a) 0, (b) 10, (c) 100, and (d) 1000 MCF-7–spiked 10-fold–diluted blood samples. (B) Relative signal intensity of the $[Au_1]^+$ ion $[(I_{Au1+}{}^0 - I_{Au1+})/I_{Au1+}{}^0]$ plotted with respect to the concentration of MCF-7 cells. $I_{Au1+}{}^0$ and I_{Au1+} represent the signal intensities of the $[Au_1]^+$ ion in the absence and presence of spiked MCF-7 cells, respectively. Error bars in B represent standard deviations from four repeated experiments. Other conditions were the same as those described in Figure 4.

fruits and vegetables; it displays has unique antioxidant, antitumor, and anti-inflammatory properties by regulating the production of some proteases, including superoxide dismutase (SOD), cyclin-dependent kinases (CDKs), and cyclooxygenase-2 (COX-2).[46] Apigenin has also been demonstrated to inhibit MUC1 gene expression and, therefore, the production of mucin protein in epithelial cells and tumor cells.[47] Through Apt_{MUC1}–Au NF/LDI-MS analysis, we also observed apigenin-induced downregulation of MUC1 expression (Figure 4e). The value of $(I_{Au+}{}^0 - I_{Au+})/I_{Au+}{}^0$ of the apigenin-treated MCF-7 cells (Figure 4Be) was not significantly different from that of the control (Figure 4Ba), revealing that MUC1 expression had indeed been downregulated after treating MCF-7 with apigenin at a concentration of 75 μM. The cell viability, assessed through an Alamar Blue assay, revealed no statistically significant difference between untreated and apigenin (75 μM)-treated cells (data not shown). The downregulation of MUC1 in MCF-7 cells was further supported by Western blotting (Figure S4, Supporting Information), revealing that our Apt_{MUC1}–Au NF/LDI-MS system has great potential for use in analyses of the expression of protein biomarkers on membranes.

We further employed the Apt_{MUC1}–Au NF/LDI-MS system for the detection of CTCs (MCF-7 cell-spiked blood samples). The signal intensities of the Au cluster ions decreased upon increasing the number of MCF-7 cells from 0 to 1000 (Figure 5A). Although $[Au_3]^+$ has the most signal intensity, as evident from Figure 4A, its signal reproducibility (RSD $\approx$ 30%) with respect to MCF-7 cells concentration is poorer than that of $[Au_1]^+$ (RSD $\approx$ 10%). Therefore, the $[Au_1]^+$ ions were monitored for the determination of cell concentration. When monitoring the $[Au_1]^+$ signals, our Apt_{MUC1}–Au NF/LDI-MS probe could detect as few as 10 MCF-7 cells (Figure 5B). In addition, analysis of the different cells ratio (MCF-7/293T cells; 0/1000, 10/990, 50/950, 100/900, 500/500, 1000/0)-spiked blood samples by Apt_{MUC1}–Au NF/LDI-MS show similar response of relative $[Au_1]^+$ signal decrease (Figure S5, Supporting Information) to MCF-7 cell alone (Figure 5B), revealing the high specificity of the Apt_{MUC1}–Au NFs. Compared with reported optical and electrochemical detecting systems for the analysis of CTCs, our Apt_{MUC1}–Au NF/LDI-MS probe is relatively simple, sensitive, selective, and capable of high throughput.[18,48−52] Notably, our Apt_{MUC1}–Au NF/LDI-MS system operates without the need for complicated agents (dyes, NPs, or electro-active organic molecules) for the labeling of targeted cells. The Au cluster ions signals decreased after modification with aptamer molecules and tumor cells binding. Future efforts could be focused on optimization of the ligands (aptamers) on Au NFs to minimize the effect of Au NFs' surface ligands and improve the detection of tumor cells.

CONCLUSIONS

We have demonstrated the general applicability of aptamer-modified Au NFs as LDI-MS matrices and as capturing probes for the detection of tumor cells in blood. The thickness of the Au NF and the laser power density both impact the transformation of Au NFs and the formation of Au cluster ions under nanosecond pulsed laser irradiation. To the best of

DOI: 10.1021/acsami.5b00731
ACS Appl. Mater. Interfaces 2015, 7, 8622−8630

our knowledge, this paper is the first to report an investigation into the formation of NPs on substrates simultaneously with the desorption and ionization of cluster ions. Our study has revealed that monitoring Au cluster ions through LDI-MS is a means of highly amplifying the measurement of the density of surface ligands on Au NFs. The decreases in the desorption and ionization efficiencies of the Au cluster ions upon increasing the density of surface DNA ligands on the Au NFs appears to be due to the ligands inhibiting electron ejection. Furthermore, we have employed an Apt_{MUC1}–Au NF chip as a capture probe for the detection, coupled with LDI-MS, of MCF-7 cells in blood samples. This Apt_{MUC1}–Au NF/LDI-MS system allows the selective detection of as few as 10 MCF-7 cells in 10-fold dilute blood sample (20 μL). The limit of detection for our method is approximately 500 tumor cells/mL, which still needs improvement for the requirement of practical use. Therefore, we will be committed to improve the limit of detection for CTCs by elementary separation of CTCs using track-etched polycarbonate membranes from blood samples in our future work. This Au NF/LDI-MS technique has great potential for application in the clinical diagnosis of tumor metastasis. The high-throughput of LDI-MS–based detection systems also suggests high applicability in array analyses of tumor cells, with the possibility of detecting other types of tumor cells and pathogens through the use of various modified metallic NFs.

■ ASSOCIATED CONTENT

Supporting Information

Table for thiolated DNA sequences and Figures S1–S5, which represent the SEM images of Au NFs, SEM images and size distribution of Au NPs formed from the T_{45}–Au $NFs_{20\ nm}$ chips after irradiation, fluorescence images for selective capture the MCF-7 by Apt_{MUC1}–Au NF, Western blotting for MUC1 in the cell lysate of MCF-7 cells, and analysis different ratio cell-spiked blood samples. This material is available free of charge via the Internet at http://pubs.acs.org.

■ AUTHOR INFORMATION

Corresponding Author

*E-mail: huanging@ntou.edu.tw. Tel.: +886-2-24622192, ext. 5517. Fax: +886-2-24622320.

Notes

The authors declare no competing financial interest.

■ ACKNOWLEDGMENTS

This study was supported by the Ministry of Science and Technology of Taiwan under contracts NSC 101-2628-M-019-001-MY3, 102-2113-M-019-001-MY3, and 102-2627-M-019-001-MY3. The assistance of Ms. Ya-Yun Yang and Ms. Ching-Yen Lin from the Instrument Center of National Taiwan University (NTU) for TEM and SEM measurements is appreciated.

■ REFERENCES

(1) Greco, A. F.; Zucca, A.; Taccola, S.; Mazzolai, B.; Mattoli, V. Patterned Free-Standing Conductive Nanofilms for Ultraconformable Circuits and Smart Interfaces. *ACS Appl. Mater. Interfaces* **2013**, *5*, 9461–9469.

(2) Wang, X.; Tian, W.; Liao, M. Y.; Bando, Y.; Golberg, D. Recent Advances in Solution-Processed Inorganic Nanofilm Photodetectors. *Chem. Soc. Rev.* **2014**, *43*, 1400–1422.

(3) Gentili, D.; Foschi, G.; Valle, F.; Cavallini, M.; Biscarini, F. Applications of Dewetting in Micro and Nanotechnology. *Chem. Soc. Rev.* **2012**, *41*, 4430–4443.

(4) Thompson, C. V. Solid-State Dewetting of Thin Films. *Annu. Rev. Mater. Res.* **2012**, *42*, 399–434.

(5) Yu, R.; Shibayama, T.; Meng, X.; Takayanagi, S.; Yoshida, Y.; Yatsu, S.; Watanabe, S. Effects of Nanosecond-Pulsed Laser Irradiation on Nanostructure Formation on the Surface of Thin Au Films on SiO_2 Glass Substrates. *Appl. Surf. Sci.* **2014**, *289*, 274–280.

(6) Singh, S. C.; Zeng, H. B. Nanomaterials and Nanopatterns Based on Laser Processing: A Brief Review on Current State of Art. *Adv. Mater.* **2012**, *4*, 368–390.

(7) Favazza, C.; Kalyanaraman, R.; Sureshkumar, R. Robust Nanopatterning by Laser-Induced Dewetting of Metal Nanofilms. *Nanotechnology* **2006**, *17*, 4229–4234.

(8) Krishna, H.; Shirato, N.; Favazza, C.; Kalyanaraman, R. Pulsed Laser Induced Self-Organization by Dewetting of Metallic Films. *J. Mater. Res.* **2011**, *26*, 154–169.

(9) Haustrup, N.; O'Connor, G. M. The Influence of Thin Film Grain Size on the Size of Nanoparticles Generated during UV Femtosecond Laser Ablation of Thin Gold Films. *Appl. Surf. Sci.* **2013**, *278*, 86–91.

(10) Madhar, N. A.; Varma, K. B. R. Spinodal Decomposition in Tellurite-Based Glasses Induced by Excimer Laser Irradiation. *J. Am. Ceram. Soc.* **2009**, *92*, 2609–2615.

(11) Bubb, D. M.; O'Malley, S. M.; Schoeffling, J.; Jimenez, R.; Zinderman, B.; Yi, S. Y. Size Control of Gold Nanoparticles Produced by Laser Ablation of Thin Films in an Aqueous Environment. *Chem. Phys. Lett.* **2013**, *565*, 65–68.

(12) Ruffino, F.; Pugliara, A.; Carria, E.; Bongiorno, C.; Spinella, C.; Grimaldi, M. G. Formation of Nanoparticles from Laser Irradiated Au Thin Film on SiO_2/Si: Elucidating the Rayleigh-Instability Role. *Mater. Lett.* **2012**, *84*, 27–30.

(13) Trice, J.; Thomas, D.; Favazza, C.; Sureshkumar, R.; Kalyanaraman, R. Pulsed-Laser-Induced Dewetting in Nanoscopic Metal Films: Theory and Experiments. *Phys. Rev. B* **2007**, *75*, 235439.

(14) Shoji, M.; Miyajima, K.; Mafuné, F. Ionization of Gold Nanoparticles in Solution by Pulse Laser Excitation as Studied by Mass Spectrometric Detection of Gold Cluster Ions. *J. Phys. Chem. C* **2008**, *112*, 1929–1932.

(15) Hashimoto, S.; Uwada, T.; Hagiri, M.; Shiraishi, R. Mechanistic Aspect of Surface Modification on Glass Substrates Assisted by Single Shot Pulsed Laser-Induced Fragmentation of Gold Nanoparticles. *J. Phys. Chem. C* **2011**, *115*, 4986–4993.

(16) Knijn, N.; Ridder, J. A M; Punt, C. J A; Wilt, J. H. W.; Nagtegaal, I. D. Histopathological Evaluation of Resected Colorectal Cancer Liver Metastases: What Should be Done? *Histopathology* **2013**, *63*, 149–156.

(17) Krebs, M. G.; Hou, J.-M.; Ward, T. H.; Blackhall, F. H.; Dive, C. Circulating Tumour Cells: Their Utility in Cancer Management and Predicting Outcomes. *Ther. Adv. Med. Oncol.* **2010**, *6*, 351–365.

(18) Costa, C.; Abal, M.; López-López, R.; Muinelo-Romay, L. Biosensors for the Detection of Circulating Tumour Cells. *Sensors* **2014**, *14*, 4856–4875.

(19) Kufe, D. W. Membrane-bound Mucins: the Mechanistic Basis for Alterations in the Growth and Survival of Cancer Cells. *Nat. Rev. Cancer* **2009**, *9*, 874–885.

(20) Ferreira, C. S.; Matthews, M. C. S.; Missailidis, S. DNA Aptamers that bind to MUC1 Tumour Marker: Design and Characterization of MUC1-binding Single-Stranded DNA Aptamers. *Tumor Biol.* **2006**, *27*, 289–301.

(21) Hua, X.; Zhou, Z. X.; Yuan, L.; Liu, S. Q. Selective Collection and Detection of MCF-7 Breast Cancer Cells Using Aptamer-Functionalized Magnetic Beads and Quantum Dots Based Nano-bio-Probes. *Anal. Chim. Acta* **2013**, *788*, 135–140.

(22) Cheng, A. K. H.; Su, H. P.; Wang, Y. A.; Yu, H.-Z. Aptamer-Based Detection of Epithelial Tumor Marker Mucin 1 with Quantum Dot-based Fluorescence Readout. *Anal. Chem.* **2009**, *81*, 6130–6139.

DOI: 10.1021/acsami.5b00731
ACS Appl. Mater. Interfaces 2015, 7, 8622–8630

(23) He, Y.; Lin, Y.; Tang, H. W.; Pang, D. W. A Graphene Oxide-based Fluorescent Aptasensor for the Turn-on Detection of Epithelial Tumor Marker Mucin 1. *Nanoscale* **2012**, *4*, 2054−2059.
(24) Lin, Z. H.; Ma, Q.; Fei, X. F.; Zhang, H.; Su, X. G. A Novel Aptamer Functionalized $CuInS_2$ Quantum Dots Probe for Daunorubicin Sensing and Near Infrared Imaging of Prostate Cancer Cells. *Anal. Chim. Acta* **2014**, *818*, 54−60.
(25) Wu, P.; Gao, Y.; Zhang, H.; Cai, C. X. Aptamer-Guided Silver−Gold Bimetallic Nanostructures with Highly Active Surface-Enhanced Raman Scattering for Specific Detection and Near-Infrared Photothermal Therapy of Human Breast Cancer Cells. *Anal. Chem.* **2012**, *84*, 7692−7699.
(26) Li, Y.-J.; Chiu, W.-J.; Unnikrishnan, B.; Huang, C.-C. Monitoring Thrombin Generation and Screening Anticoagulants through Pulse Laser-Induced Fragmentation of Biofunctional Nanogold on Cellulose Membranes. *ACS Appl. Mater. Interfaces* **2014**, *6*, 15253−15261.
(27) Petrovykh, D. Y.; Kimura-Suda, H.; Whitman, L. J.; Tarlov, M. J. Quantitative Analysis and Characterization of DNA Immobilized on Gold. *J. Am. Chem. Soc.* **2003**, *125*, 5219−5226.
(28) Ruffino, F.; Grimaldi, M. G. Atomic Force Microscopy Study of the Growth Mechanisms of Nanostructured Sputtered Au Flm on Si(111): Evolution with Film Thickness and Annealing Time. *J. Appl. Phys.* **2010**, *107*, 104321.
(29) Nedyalkov, N. N.; Nikov, R.; Dikovska, A. O.; Atanasov, P. A.; Obara, G.; Obara, M. Laser Annealing of Bimetal Thin Films: A Route of Fabrication of Composite Nanostructures. *Appl. Surf. Sci.* **2012**, *258*, 9162−9166.
(30) Ratautas, K.; Gedvilas, M.; Račiukaitis, G.; Grigonis, A. Nanoparticle Formation after Nanosecond-Laser Irradiation of Thin Gold Films. *J. Appl. Phys.* **2012**, *112*, 013108.
(31) Ruffino, F.; Pugliara, A.; Carria, E.; Romano, L.; Bongiorno, C.; Spinella, C.; Grimaldi, M. G. Novel Approach to the Fabrication of Au/Silica Core−Shell Nanostructures based on Nanosecond Laser Irradiation of Thin Au Films on Si. *Nanotechnology* **2012**, *23*, 045601.
(32) Ratautas, K.; Gedvilas, M.; Voisiat, B.; Račiukaitis, G.; Grigonis, A. Transformation of a Thin Gold Film to Nanoparticles after Nanosecond−Laser Irradiation. *J. Laser Micro/Nanoeng.* **2012**, *7*, 355−361.
(33) Kim, H. S.; Wood, T. D.; Marshall, A. G.; Lee, J. Y. Production of Gold Cluster Ions by Laser Desorption/Ionization Fourier-transform Ion Cyclotron Resonance Mass Spectrometry. *Chem. Phys. Lett.* **1994**, *224*, 589−594.
(34) Hashimoto, S.; Werner, D.; Uwada, T. Studies on the Interaction of Pulsed Lasers with Plasmonic Gold Nanoparticles toward Light Manipulation, Heat Management, and Nanofabrication. *J. Photochem. Photobiol., C* **2012**, *13*, 28−54.
(35) Yamada, K.; Miyajima, K.; Mafune, F. Thermionic Emission of Electrons from Gold Nanoparticles by Nanosecond Pulse-Laser Excitation of Interband. *J. Phys. Chem. C* **2007**, *111*, 11246−11251.
(36) Qiu, T. Q.; Tien, C.-L.; Shannon, M. A. Thermal and Mechanical Responses of Gold Films during Nanosecond Laser Pulse Heating. *Exp. Heat Transfer* **1994**, *7*, 175−188.
(37) Mao, Y. J.; Zhang, Y. W.; Chen, J. K. Melting, Vaporization, and Resolidification in a Thin Gold Film Irradiated by Multiple Femtosecond Laser Pulses. *J. Manuf. Sci. Eng.* **2013**, *135*, 021007.
(38) Liu, Y.-C.; Li, Y.-J.; Huang, C.-C. Information Derived from Cluster Ions from DNA-Modified Gold Nanoparticles under Laser Desorption/Ionization: Analysis of Coverage, Structure, and Single-Nucleotide Polymorphism. *Anal. Chem.* **2013**, *85*, 1021−1028.
(39) Chiang, C.-K.; Chen, W.-T.; Chang, H.-T. Nanoparticle-Based Mass Spectrometry for the Analysis of Biomolecules. *Chem. Soc. Rev.* **2011**, *40*, 1269−1281.
(40) Dong, X.; Cheng, J.; Li, J.; Wang, Y. Graphene as a Novel Matrix for the Analysis of Small Molecules by MALDI-TOF MS. *Anal. Chem.* **2010**, *82*, 6208−6214.
(41) Tang, H.-W.; Wong, M. Y.-M.; Lam, W.; Cheng, Y.-C.; Che, C.-M.; Ng, K.-M. Gold Nanomaterials as a New Tool for Bioanalytical Applications of Laser Desorption Ionization Mass Spectrometry. *Rapid Commun. Mass Spectrom.* **2011**, *25*, 3690−3696.
(42) Cha, S.; Song, Z.; Nikolau, B. J.; Yeung, E. S. Direct Profiling and Imaging of Epicuticular Waxes on Arabidopsis thaliana by Laser Desorption Ionization Mass Spectrometry Using Silver Colloid as a Matrix. *Anal. Chem.* **2009**, *81*, 2991−3000.
(43) Chen, Z.; Geng, Z.; Shao, D.; Mei, Y.; Wang, Z. Single-Crystalline EuF3 Hollow Hexagonal Microdisks Synthesis and Application as a Background-Free Matrix for MALDI-TOF-MS Analysis of Small Molecules and Polyethylene Glycols. *Anal. Chem.* **2009**, *81*, 7625−7631.
(44) Nath, S.; Mukherjee, P. MUC1: a Multifaceted Oncoprotein with a Key Role in Cancer Progression. *Trends Mol. Med.* **2014**, *20*, 332−342.
(45) Rahn, J. J.; Shen, Q.; Mah, B. K.; Hugh, J. C. MUC1 Initiates a Calcium Signal after Ligation by Intercellular Adhesion Molecule-1. *J. Biol. Chem.* **2004**, *279*, 29386−29390.
(46) Patel, D.; Shukla, S.; Gupta, S. Apigenin and Cancer Chemoprevention: Progress, Potential and Promise. *Int. J. Oncol.* **2007**, *30*, 233−245.
(47) Zhou, Y. C.; Rajabi, H. S.; Kufe, D. Mucin 1 C-Terminal Subunit Oncoprotein Is a Target for Small-Molecule Inhibitors. *Mol. Pharmacol.* **2011**, *79*, 886−893.
(48) Joosse, S. A.; Pantel, K. Biologic Challenges in the Detection of Circulating Tumor Cells. *Cancer Res.* **2013**, *73*, 8−11.
(49) Esmaeilsabzali, H.; Beischlag, T. V.; Cox, M. E.; Parameswaran, A. M.; Park, E. J. Detection and Isolation of Circulating Tumor Cells: Principles and Methods. *Biotechnol. Adv.* **2013**, *31*, 1063−1084.
(50) Hajba, L.; Guttman, A. Circulating Tumor-Cell Detection and Capture Using Microfluidic devices. *Trends. Anal. Chem.* **2014**, *59*, 9−16.
(51) Sun, Y.-F.; Yang, X.-R.; Zhou, J.; Qiu, S.-J.; Fan, J.; Xu, Y. Circulating Tumor Cells: Advances in Detection Methods, Biological Issues, and Clinical Relevance. *J. Cancer Res. Clin. Oncol.* **2011**, *137*, 1151−1173.
(52) Alix-Panabièresab, C.; Pantel, K. Technologies for Detection of Circulating Tumor Cells: Facts and Vision. *Lab Chip* **2014**, *14*, 57−62.

DOI: 10.1021/acsami.5b00731
ACS Appl. Mater. Interfaces 2015, 7, 8622−8630